Electronic Supplementary Information

Electronic Structure Modulation with Single Atoms Interficial Engineering for Selective Atmospheric CO_2 Photoreduction

Yangzi Shangguan [a], Fuping Li [b], Xuezhen Feng [a], Ranhao Wang [a], Qiuyue Ge [a], Xiaoyong Wu [*b], Hong Chen [*a]

[a] State Environmental Protection Key Laboratory of Integrated Surface Water-Groundwater Pollution Control, School of Environmental Science and Engineering, Guangdong Provincial Key Laboratory of Soil and Groundwater Pollution Control, Southern University of Science and Technology, Shenzhen, Guangdong 518055, China.

[b] Hubei Key Laboratory of Mineral Resources Processing and Environment, School of Resources and Environmental Engineering, Wuhan University of Technology, Wuhan, 430070, China

*Corresponding author: H. Chen (chenh3@sustech.edu.cn),

X. Wu (parawu521@whut.edu.cn).

S1 Experimental section

1.1 Materials

Chloroplatinic acid ($H_2IrCl_6·6H_2O$, 99%), iron chloride anhydrous ($FeCl_2$, 97%), copper acetate ($Cu(CH_3COO)_2$, 98%), 1–octadecene (ODE, technical grade, 90%), oleylamine (OAm, technical grade, 70%), 1–dodecanethiol (DDT) were purchased from Aladdin Industrial Corporation (Shanghai, China). All the chemicals were used as received without further purification.

1.2 Synthesis of $CuFeS_2$ QDs

$FeCl_2$ (1 mmol) and $Cu(CH_3COO)_2$ (1 mmol) were dissolved in a 250 mL three-necked round-bottom flask equipped with ODE (20 mL) and OAm (20 mL). The solution was mixed under vigorously stirring for 1 h in a vacuum with Schenlk line. Later the reaction mixture was heated at 100 °C under vacuum for 1 h to remove water. The temperature was further increased to 120 °C with a stirring speed of 400 rpm for 1 h under argon (Ar) to dissolve the metal precursors completely. When the color of the solution turned brown, 15 mL DDT was rapidly injected into the reaction mixture. Subsequently, the temperature was increased to 235 °C and maintained for another 1 h to initiate the nucleation of $CuFeS_2$ QDs. When the color of the solution turned into atropurpureus, the heating mantle was removed. The mixture was cooled down to room temperature. Finally, the obtained dark suspension was washed with acetone and methanol four times, then centrifuged and dried in air at 80 °C for 12 h. The $CuFeS_2$ QDs powders were harvested.

1.3 Synthesis of Ir/$CuFeS_2$

Typically, the as-prepared $CuFeS_2$ QDs (80 mg) were added into a 100 mL flask with 50 mL $H_2IrCl_6·6H_2O$ solution (10 mg/L) and stirred under sunlight irradiation at room temperature for 12 h. The resulting product was washed carefully with deionized (DI) water under ultraviolet lamp illumination and dried in a vacuum oven at 60 °C for 12 h. Subsequently, the reaction mixture was heated to 450 °C in a tube furnace with a heating rate of 5 °C/min and maintain for 3 h under sulfur vapor. After cooling down to room temperature, Ir decorated $CuFeS_2$ QDs denoted as Ir/$CuFeS_2$ were harvested.

1.4 Photocatalytic CO_2 reduction tests

Photocatalysis experiments were conducted in a custom-made glass vessel equipped with a quartz glass cap (Perfectlight, China). A 300 W Xe lamp (Perfectlight, China) served as the full spectrum light source, while visible light was obtained by using a 420 nm filter to exclude UV light. A relatively low

concentration of CO_2 (approximately 1500 ppm) was generated in situ for the standard catalysis reaction by reacting $NaHCO_3$ with H_2SO_4 (in a 1:1 volume ratio of concentrated H_2SO_4 and deionized water). The in-house atmospheric air, containing approximately 500 ppm of CO_2 as determined by gas chromatography, was also used as a CO_2 source for photocatalytic CO_2 reduction.

The following procedures were followed: 25 mg of the photocatalyst was uniformly dispersed in 1 mL of deionized water and then dried in a 60 °C oven. Subsequently, 50 µL of deionized water was added to the catalyst's surface to create a humid interface. Next, 500 mg of $NaHCO_3$ was added to a 200 mL glass reaction chamber, followed by the placement of the prepared sample vessel on top of the $NaHCO_3$ powder. The reaction chamber was then purged with pure N_2 gas for 30 minutes to remove air and then evacuated for 15 minutes. Before light irradiation, 2 mL of H_2SO_4 was injected into the reaction chamber to initiate the production of a low concentration of CO_2. At regular intervals, 200 µL of the gas products were withdrawn and qualitatively analyzed using gas chromatography.

The $^{13}CO_2$ photoreduction experiment was also conducted in a customized glass vessel using a $^{13}CO_2$ source produced by reacting $NaH^{13}CO_3$ with H_2SO_4.

1.5 Instrumental characterization

The residual Ir concentration in the supernatant was measured with inductive coupled plasma mass spectrometry (ICP-MS) with a Thermo ICAP RQ instrument, in which the elemental mass analysis range was 2–290 (AMU). High-angle annular dark-field scanning transmission electron microscope (HAADF-STEM) and energy-dispersive X-ray spectroscopy (EDS) elemental analysis were performed on an FEI Titan Themis apparatus with an X-FEG electron gun and a DCOR aberration corrector operating at 300 kV. For the TEM sample preparation, Ir/$CuFeS_2$ powders were dispersed in n-hexane and then dropped cast onto the carbon-coated 200 mesh nickel grids. Powder X-ray diffraction (PXRD) analysis was performed on a Rigaku Smart-Lab 9 kW diffractometer with the X-ray tube operated at 45 kV and 20 mA in the 2ϑ ranging from 20° to 70° with a scan rate of 0.02° per second. X-ray photoelectron spectrometer (XPS) data were recorded with PHI 5000 Versaprobe III equipped with a monochromatic Al anode (Al Kα = 1486.7 eV) source. Valence state analyses of the samples before and after Ir were carried with the software MultiPak [1]. All binding energies (BE) were referenced to the C1s peak arising from the background carbon. The ultraviolet-visible diffuse reflectance spectra (UV-Vis DRS) of the samples were collected using a Shimadzu UV–3600 PC spectrophotometer with $BaSO_4$ as the reference material. The data has been converted into the Tauc plot according to the Kubelka–Munk method[2] by

the following equation 1 (Eq. 1):

$$\alpha h\nu = A\,(h\nu - E_g)^{1/2} \quad (1)$$

where A is a constant, α, $h\nu$, and E_g are the absorption coefficient, the photon energy, and the direct bandgap, respectively.

1.6 Mott-Schottky curve measurements

The Mott-Schottky curve was tested in Na_2SO_4 solution of a certain concentration. The specific test methods are as follows. Configuration of 1 mol/L Na_2SO_4 solution, 20 mg $CuFeS_2$ and Ir/$CuFeS_2$ QDs dispersed in 5 ml ethanol. After ultrasonic dispersion, the mixture was dripped in the conductive glass. After drying, the sample can be tested (the sample preparation must be uniform and as thin as possible). Samples can be ground before the ultrasound. Three-electrode system test showed that the electrolyte was Na_2SO_4 solution; the reference electrode was Ag/AgCl electrode, the Ir mesh electrode and the working electrode were conductive glass with the sample to be measured. In a certain voltage range (1 V *vs* Ag/AgCl), the test frequency was changed (generally 500, 1000, 1500 Hz). The result of the test is flat-band potential (E_v). For n-type semiconductor, its conduction band potential is ~0.1 V smaller than its flat-band, and the standard potential of Ag/AgCl has a potential difference of ~0.197 V relative to the standard hydrogen potential.[3, 4]

1.7 Electrochemical impedance spectroscopy (EIS) measurements

The EIS Nyquist plot was tested in Na_2SO_4 solution of a certain concentration. The specific test methods are as follows. Configuration of 1 M Na_2SO_4 solution, 20 mg $CuFeS_2$ and Ir/$CuFeS_2$ QDs dispersed in 5 ml ethanol. After ultrasonic dispersion, the mixture was dripped in the conductive glass. After drying, the sample can be tested (the sample preparation must be uniform and as thin as possible). Samples can be ground before the ultrasound. Three-electrode system test showed that the electrolyte was Na_2SO_4 solution; the reference electrode was Ag/AgCl electrode, the platinum mesh electrode and the working electrode were conductive glass with the sample to be measured. The test frequency was 100000−0.01 Hz with a 5 mV amplitude.

1.8 Density functional theory (DFT) calculations

For the density functional theory (DFT) calculations, the electron exchange-correlation potential was conducted by the Perdew-Burke-Ernzerhof (PBE) functional of generalized gradient approximation (GGA), and the ultrasoft pseudopotentials were employed. [5] To simulate the adsorption of Ir atom,

$CuFeS_2$ (112), the preferred exposure crystallographic plane as suggested from powder XRD characterization, was constructed by a periodic four-layer slab with a vacuum region of 15 Å along with the *z*-axis. DFT+U methord[6] with an effective on-site Hubbard U_{eff} correction, was employed to describe the d electrons for the transition metals in our system. DFT-D was used to describe the van der Waals interactions. Brillouin zone integration was sampled with 4 × 4 × 1 Monkhorst Pack mesh *k*-point for the surface model, and an energy cutoff of 550 eV was applied for the plan-wave basis set. The convergence tolerances were set to 1×10^{-5} eV per atom for energy, 1×10^{-3} Å for maximum displacement, and 0.03 eV/Å for maximum force. The adsorption energy (E_{ads}) of Ir on the $CuFeS_2$ surface was calculated as follows:

$$E_{ads} = E_{Surf + Ir} - E_{Surf} - E_{Ir} \quad (2)$$

where $E_{Surf + Ir}$ is the total energy of $CuFeS_2$ (112) slab adsorbed with Ir, E_{Surf} is the energy of the $CuFeS_2$ (112) slab with a clean surface and E_{Ir} is the energy of the Ir atom.

The Gibbs free energy change (Δ*G*) for each basic step is defined as:

$$\Delta G = \Delta E + \Delta ZPE - T\Delta S + \Delta G_U + \Delta G_{pH} \quad (3)$$

where Δ*E* and Δ*ZPE* are the adsorption energy based on density functional theory calculations and the zero-point energy correction, respectively. *T*, *ΔS*, *U*, and ΔG_{pH} represent the temperature, the entropy change, the applied electrode potential, and the free energy correction of the pH, respectively.

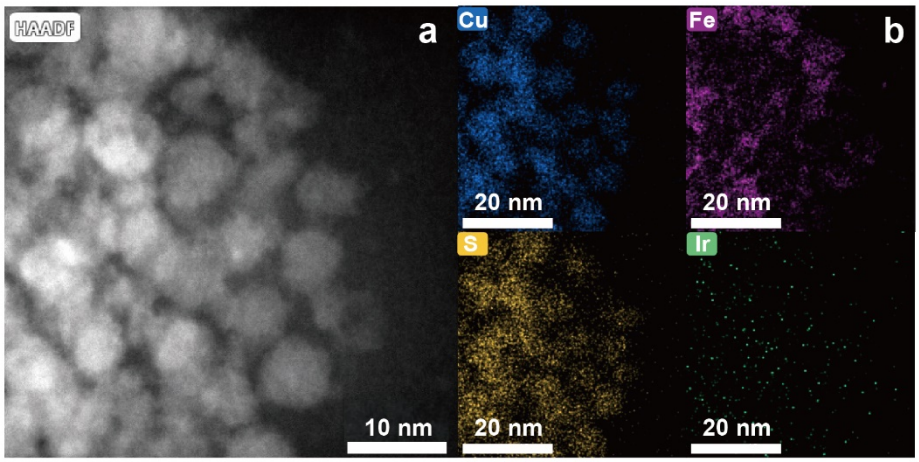

Fig. S1 Morphology and structure of Ir/$CuFeS_2$ QDs. (a) HAADF-STEM image of Ir/$CuFeS_2$. (b) EDS mapping of element distribution of Fe, Cu, S, Ir.

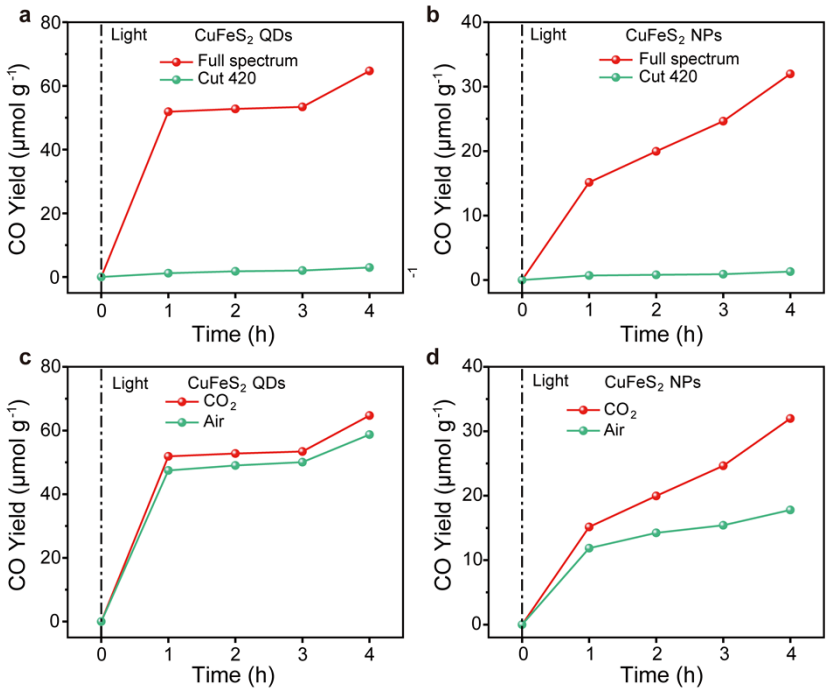

Fig. S2 CO_2 photoreduction performance under different reaction conditions over $CuFeS_2$ QDs and $CuFeS_2$ NPs. CO_2 photoreduction performance over (a) $CuFeS_2$ QDs and (b) $CuFeS_2$ NPs under different spectrum light irradiation. CO_2 photoreduction performance over (c) $CuFeS_2$ QDs and (d) $CuFeS_2$ NPs under different atmosphere.

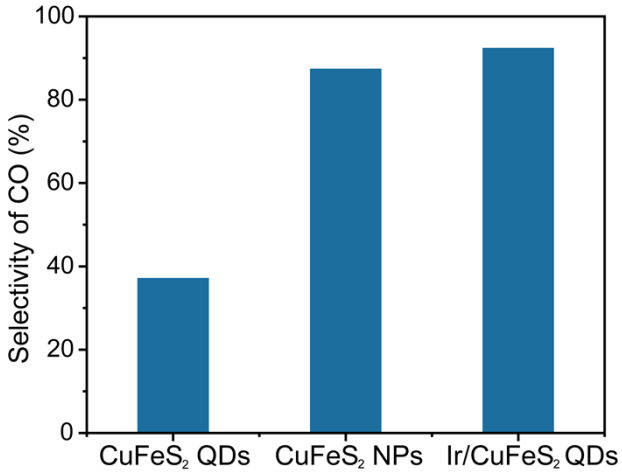

Fig. S3 Selectivity of CO_2 reduction to CO with $CuFeS_2$ NPs, $CuFeS_2$ QDs and Ir/$CuFeS_2$ QDs.

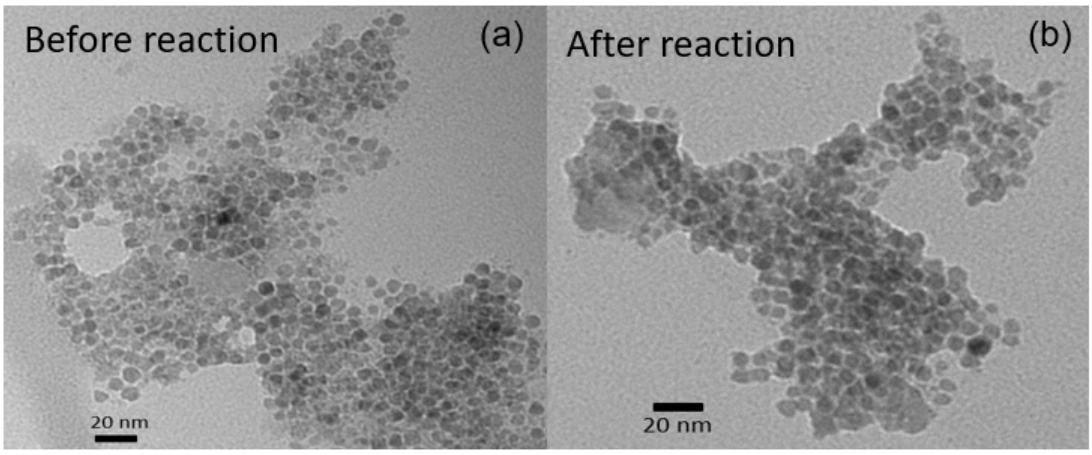

Fig. S4 The change of Ir/$CuFeS_2$ QDs morphology (a) before and (b) after reaction.

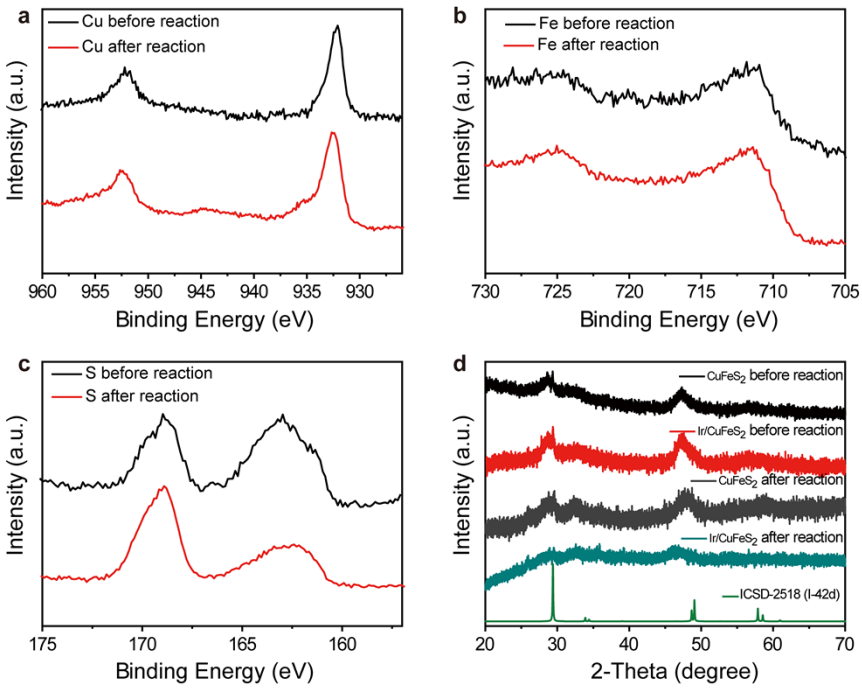

Fig. S5 Experimental data of CO_2 reduction mechanism. XPS of (a) Cu, (b) Fe , (c) S, and (d) XRD of Ir/$CuFeS_2$ QDs before and after the reaction.

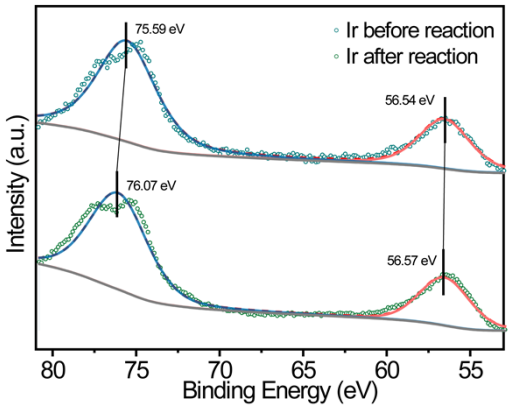

Fig. S6 High-resolution XPS of Ir in Ir/$CuFeS_2$ QDs before and after the reaction.

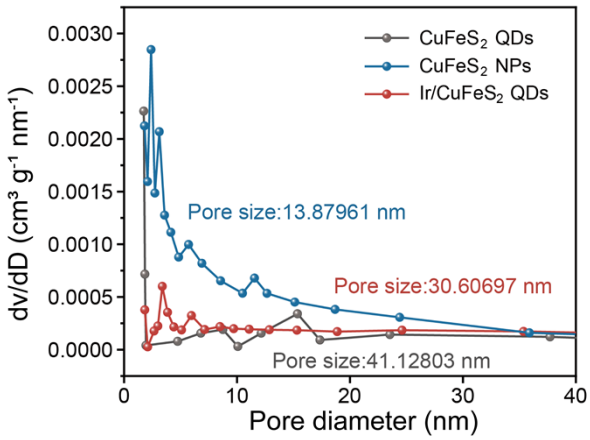

Fig. S7 Pore size distribution of $CuFeS_2$ NPs, $CuFeS_2$ QDs and Ir/$CuFeS_2$ QDs.

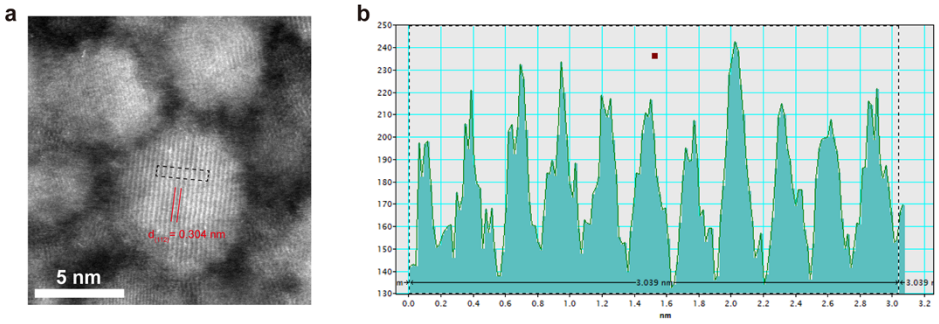

Fig. S8 (a) Aberration-corrected HAADF-STEM image of Ir/$CuFeS_2$ QD. (b) Lattice spacing analysis of the square marked with black dots.

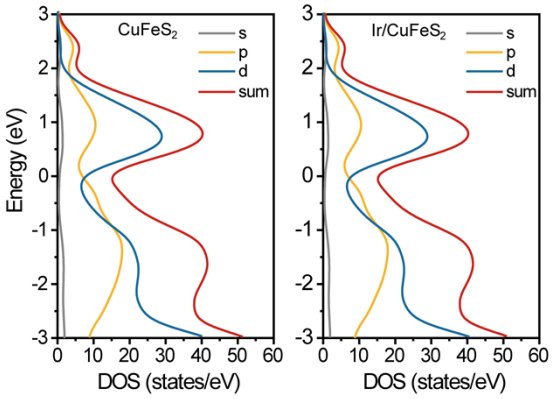

Fig. S9 Partial density of states (PDOS) of $CuFeS_2$ QDs and Ir/$CuFeS_2$ QDs.

Table S1 Iridium loading of Ir/$CuFeS_2$ determined by inductively coupled plasma atomic emission spectrometry (ICP-MS).

Element	MY_x	Metal Concentration in $M_1/CuFeS_2$ (wt %)
Ir	$H_2IrCl_6{\cdot}6H_2O$	0.06

Table S2. EXAFS fitting parameters at the Ir K-edge for various samples. (S_0^2=0.86)

Sample	Shell	N^a	R(Å)^b	$\sigma^2\times10^3$(Å^2)^c	ΔE_0 (eV)^d	R factor
Ir foil	Ir–Ir	12	2.71	2.7	8.7	0.007
IrO_2	Ir–O	4	1.64	6.5	10.6	0.016
Ir /$CuFeS_2$	Ir–S	6	1.89	9.3	8.6	0.004

[a]N: coordination numbers; [b]R: bond distance; [c]σ^2: Debye-Waller factors; [d]ΔE_0: the inner potential correction; R factor: goodness of fit.

Table S3. Comparison of CO_2 photoreduction performance with other photocatalysts.

Photocatalysts	Products	Yield (μmol g^{-1} h^{-1})	Ref.
Bi_2WO_6	CO	26.6	[7]
VBi-O-Bi_2MoO_6	CO	3.62	[8]
ZnAl-LDH	CO	7.6	[9]
V_{Zn}-poor $ZnIn_2S_4$	CO	9.22	[10]
$CuInS_2$/Re QDs	CO	2.71	[11]
Cu/ TiO_2/$BiVO_4$-4	CO	17.33	[12]
B/CAL-2	CO	20.5	[13]
$CuInS_2$ QDs	CO	4.43	[14]
Ir/$CuFeS_2$ QDs	CO	32.5	This work

Table S4. Adsorption energies E_{ads} (eV) of CO_2 on $CuFeS_2$ and Ir/$CuFeS_2$ surfaces.

Adsorption site	E_{ads} **(eV)**
$CuFeS_2$	–0.03
Ir/$CuFeS_2$	-1.67

References

1 I. S. Zhidkov, R. N. Maksimov, A. I. Kukharenko, L. D. Finkelstein, S. O. Cholakh, V. V. Osipov and E. Z. Kurmaev, *Mendeleev Commun.*, 2019, **29**, 102–104.

2 D. W. Su, J. Ran, Z. W. Zhuang, C. Chen, S. Z. Qiao, Y. D. Li and G. X. Wang, *Sci. Adv.*, 2020, **6**, 8447–8462.

3 A. Ishikawa, T. Takata, J. N. Kondo, M. Hara, H. Kobayashi and K. Domen, *J. Am. Chem. Soc.*, 2002, **124**, 13547–13553.

4 L. Yu, G. Li, X. Zhang, X. Ba, G. Shi, Y. Li, P. K. Wong, J. C. M. Yu and Y. Yu, *ACS Catal.*, 2016, **6**, 6444–6454.

5 J. P. Perdew, K. Burke and M. Ernzerhof, Phys. *Rev. Lett.*, 1996, **77**, 3865–3868.

6 Q. Ge, X. Feng, R. Wang, R. Zheng, S. Luo, L. Duan, Y. Ji, J. Lin and H. Chen, *Environ. Sci. Technol.*, 2020, **54**, 8022–8031.

7 S. Xiong, S. Bao, W. Wang, J. Hao, Y. Mao, P. Liu, Y. Huang, Z. Duan, Y. Lv and D. Ouyang, *Appl. Catal. B Environ.*, 2022, **305**, 121026.

8 J. Di, X. Zhao, C. Lian, M. Ji, J. Xia, J. Xiong, W. Zhou, X. Cao, Y. She, H. Liu, K. P. Loh, S. J. Pennycook, H. Li and Z. Liu, *Nano Energy*, 2019, **61**, 54–59.

9 Y. Zhao, G. Chen, T. Bian, C. Zhou, G. I. N. Waterhouse, L. Z. Wu, C. H. Tung, L. J. Smith, D. O'Hare and T. Zhang, *Adv. Mater.*, 2015, **27**, 7824–7831.

10 X. Jiao, Z. Chen, X. Li, Y. Sun, S. Gao, W. Yan, C. Wang, Q. Zhang, Y. Lin, Y. Luo and Y. Xie, *J. Am. Chem. Soc.*, 2017, **139**, 7586–7594.

11 J. Huang, M. G. Gatty, B. Xu, P. B. Pati, A. S. Etman, L. Tian, J. Sun, L. Hammarström and H. Tian, *Dalt. Trans.*, 2018, **47**, 10775–10783.

12 C. Chen, M. Wu, Y. Xu, C. Ma, M. Song and G. Jiang, J. Am. Chem. Soc., 2024, 146, 9163–9171.

13 J. Li, G. Gao, Y. Liu, Y. Li and Z. Liu, *J. CO_2 Util.*, 2022, **65**, 102257.

14 M. Cai, X. Tong, P. Liao, S. Shen, H. Zhao, X. Li, L. Xia, H. Zhi, N. Zhou, Z. Xue, L. Jin, J. Li, G. Li, F. Dong, A. V. Kabashin and Z. M. Wang, *ACS Catal.*, 2023, **13**, 15546–15557.